HEART DISEASE

Recruited macrophages elicit atrial fibrillation

Maarten Hulsmans[1,2]*†, Maximilian J. Schloss[1,2]†, I-Hsiu Lee[1,2]†, Aneesh Bapat[3], Yoshiko Iwamoto[1,2], Claudio Vinegoni[1,2], Alexandre Paccalet[1,2], Masahiro Yamazoe[1,2], Jana Grune[1,2], Steffen Pabel[1,2,4], Noor Momin[1,2], Hana Seung[1,2], Nina Kumowski[1,2], Fadi E. Pulous[1,2], Daniel Keller[5], Constanze Bening[5], Ursula Green[6], Jochen K. Lennerz[6], Richard N. Mitchell[7], Andrew Lewis[8,9], Barbara Casadei[8,9], Oriol Iborra-Egea[10], Antoni Bayes-Genis[10], Samuel Sossalla[4,11], Chin Siang Ong[12,13], Richard N. Pierson[12], Jon C. Aster[7], David Rohde[1,2], Gregory R. Wojtkiewicz[1,2], Ralph Weissleder[1,2], Filip K. Swirski[14,15], George Tellides[13], George Tolis Jr.[16], Serguei Melnitchouk[12], David J. Milan[17], Patrick T. Ellinor[3,18], Kamila Naxerova[1,2]*‡, Matthias Nahrendorf[1,2,3,19]*‡

Atrial fibrillation disrupts contraction of the atria, leading to stroke and heart failure. We deciphered how immune and stromal cells contribute to atrial fibrillation. Single-cell transcriptomes from human atria documented inflammatory monocyte and SPP1+ macrophage expansion in atrial fibrillation. Combining hypertension, obesity, and mitral valve regurgitation (HOMER) in mice elicited enlarged, fibrosed, and fibrillation-prone atria. Single-cell transcriptomes from HOMER mouse atria recapitulated cell composition and transcriptome changes observed in patients. Inhibiting monocyte migration reduced arrhythmia in Ccr2−/− HOMER mice. Cell-cell interaction analysis identified SPP1 as a pleiotropic signal that promotes atrial fibrillation through cross-talk with local immune and stromal cells. Deleting Spp1 reduced atrial fibrillation in HOMER mice. These results identify SPP1+ macrophages as targets for immunotherapy in atrial fibrillation.

In healthy atria, excitations arising in the sinus node coordinate atrial contractions that help fill the ventricles in diastole. Cardiomyocytes constitute 30% of atrial cells (1). The remaining 70% of atrial cells are fibroblasts, endothelial cells, and resident immune cells. Together, these provide cardiomyocytes with housekeeping functions, including matrix scaffold, blood supply, waste removal, and immunosurveillance (2, 3). Atrial fibrillation (AFib) is the most common arrhythmia (4). During AFib, the lack of coordinated atrial excitation and contraction slows blood flow into the ventricles. This sluggishness can diminish cardiac performance and give rise to atrial blood clots that cause thromboembolic stroke.

Inflammation may contribute to AFib through electrical remodeling (5–7), during which altered ion handling perturbs the action potential (8). Fibrosis, another consequence of inflammation, induces heterogeneous atrial depolarization, which provides an opportunity for electrical conduction reentry and subsequent AFib (8, 9). To examine how immune and stromal cells contribute to AFib, we performed single-cell RNA sequencing (scRNA-seq) of freshly isolated normal and diseased human atrial tissue.

Macrophages expand in human atrial disease

We collected left atrial tissue from five control participants and seven patients with persistent AFib undergoing heart surgery (table S1) and performed scRNA-seq on the 10X Genomics Chromium platform (Fig. 1A and fig. S1A). A total of 41,609 viable, single cells from both patients with AFib and controls were partitioned into clusters (fig. S1B), which we annotated using known lineage markers (fig. S1C). We identified six major noncardiomyocyte cell types, which included (in order of decreasing frequency) lymphocytes, mononuclear phagocytes and dendritic cells (MP/DCs), endothelial cells, fibroblasts, mural cells, and neutrophils (Fig. 1, B and C; fig. S2; and table S2).

In diseased atria, the MP/DC cluster expanded twofold, whereas endothelia and mural cells decreased in frequency. The other cell classes remained stable (Fig. 1C and table S2). Because the MP/DC cluster increased considerably, we scrutinized the transcriptomes of these cells more closely. We identified genes that were differentially expressed in MP/DCs from AFib and control atria with a pseudo-bulk approach that aggregated cells from the same individual to determine differential gene expression between the two patient groups (10). We then performed gene set enrichment analysis (GSEA) (11) on the resulting list of differentially expressed genes to define the pathways and functional gene groups that were altered in MP/DCs from patients with AFib. In this disease setting, MP/DCs up-regulated gene sets related to the inflammatory response, interferon-γ (IFN-γ) signaling, monocyte recruitment, and cholesterol metabolism (Fig. 1D and data S1). Thus, atrial MP/DCs undergo substantial immunometabolic remodeling during their expansion in patients with AFib.

To gain a broader understanding of the transcriptional programs that are activated or repressed in MP/DCs, we used weighted correlation network analysis to study groups of correlated genes that were differentially expressed between patients and controls (12). We identified 24 modules of correlated genes across all participants, three of which were significantly correlated with disease state. Module 1 was up-regulated in AFib and contained inflammatory and profibrotic genes such as CCR2, IL10, ITGA9, MMP9, SPP1, TIMP2, and VIM (Fig. 1E and data S2) (13–15). Overrepresentation analysis confirmed that inflammatory and extracellular matrix–related gene sets characterized module 1 (Fig. 1F and data S2). Module 1 genes SPP1 and CCR2 and the cell surface markers TREM2 and CD9 were among the top up-regulated genes in MP/DCs from patients with AFib (Fig. 1G). SPP1 encodes the matricellular protein osteopontin, which participates in bone remodeling and fibrosis by promoting cell survival, adhesion, and migration as well as inflammatory cell activation (13). The chemokine receptor CCR2 mediates monocyte egress from the bone marrow (16) and is essential for monocyte recruitment (14). Gene modules 2 and 3, whose expression was down-regulated in MP/DCs from patients with AFib, included genes involved in protecting against cardiac disease [SIRT2 (17)], cardiac resident macrophage proliferation [KLF4 (18)], and epigenetic constraint of cytokine production [HDAC2 (19) and ODC1 (20)] (Fig. 1E and data S2). These data imply that the atria of patients with AFib have elevated numbers of myeloid cells that assume a more inflammatory phenotype, implicating macrophages in the tissue remodeling that disrupts coordinated excitation of atrial cardiomyocytes. Other leukocytes and stromal

[1]Center for Systems Biology, Massachusetts General Hospital and Harvard Medical School, Boston, MA, USA. [2]Department of Radiology, Massachusetts General Hospital and Harvard Medical School, Boston, MA, USA. [3]Cardiovascular Research Center, Massachusetts General Hospital and Harvard Medical School, Boston, MA, USA. [4]Department of Internal Medicine II, University Medical Center Regensburg, Regensburg, Germany. [5]Department of Thoracic and Cardiovascular Surgery, University Hospital Wuerzburg, Wuerzburg, Germany. [6]Department of Pathology, Center for Integrated Diagnostics, Massachusetts General Hospital and Harvard Medical School, Boston, MA, USA. [7]Department of Pathology, Brigham and Women's Hospital and Harvard Medical School, Boston, MA, USA. [8]Radcliffe Department of Medicine, NIHR Biomedical Research Centre, University of Oxford, Oxford, UK. [9]British Heart Foundation Centre of Research Excellence, University of Oxford, Oxford, UK. [10]Institut del Cor Germans Trias i Pujol, CIBERCV, Badalona, Barcelona, Spain. [11]Department of Cardiology and Angiology, University of Giessen/DZHK, Partner Site Rhein-Main, Germany. [12]Division of Cardiac Surgery, Massachusetts General Hospital and Harvard Medical School, Boston, MA, USA. [13]Department of Surgery, Yale School of Medicine, New Haven, CT, USA. [14]Cardiovascular Research Institute, Icahn School of Medicine at Mount Sinai, New York, NY, USA. [15]Department of Medicine, Icahn School of Medicine at Mount Sinai, New York, NY, USA. [16]Department of Cardiac Surgery, Brigham and Women's Hospital and Harvard Medical School, Boston, MA, USA. [17]Leducq Foundation, Boston, MA, USA. [18]Cardiovascular Disease Initiative, The Broad Institute of MIT and Harvard University, Cambridge, MA, USA. [19]Department of Internal Medicine I, University Hospital Wuerzburg, Wuerzburg, Germany.

*Corresponding author. Email: mhulsmans@mgh.harvard.edu (M.H.); naxerova.kamila@mgh.harvard.edu (K.N.); mnahrendorf@mgh.harvard.edu (M.N.)

†These authors contributed equally to this work.
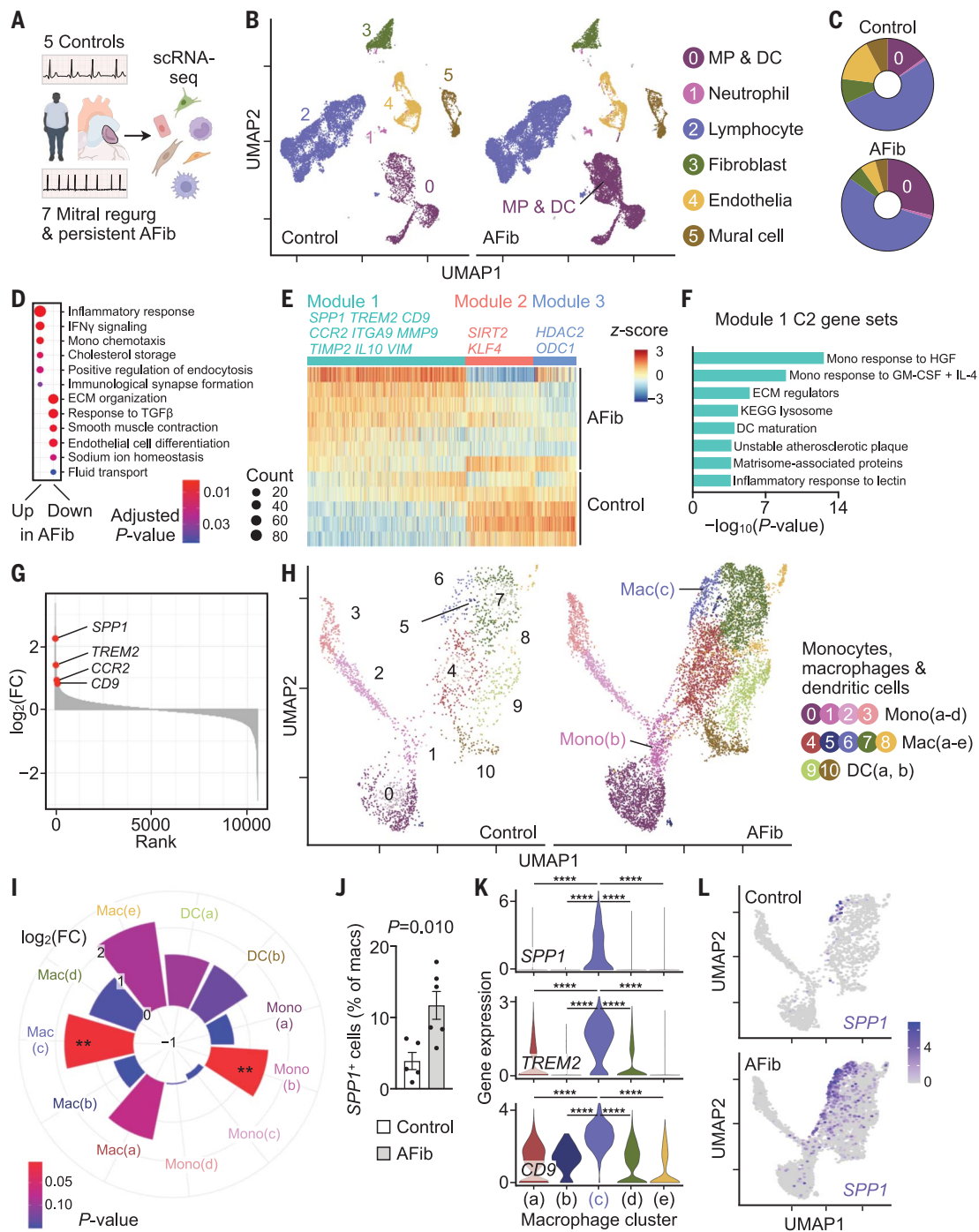‡These authors contributed equally to this work.

Fig. 1. Single-cell atlas of human atrial disease. (**A**) scRNA-seq was performed in five controls and seven patients with AFib. (**B**) UMAP delineates six major cardiac cell types. (**C**) Distribution of cell populations. Color code corresponds to (B). (**D**) Gene ontology biological process (GOBP) gene sets (*48, 49*) up- or down-regulated in AFib from GSEA of MP/DC cluster. Circle size denotes number of enriched genes. ECM, extracellular matrix. (**E**) Gene expression in MP/DC cluster represented by z-scores of the log-transformed normalized counts. Rows, samples grouped by disease state; columns, genes in the three gene modules significantly associated with disease state. Gene coexpression modules and exemplary genes are labeled. (**F**) Select MSigDB C2 gene sets (*50*) overrepresented in module 1 described in (E). GM-CSF, granulocyte-macrophage colony-stimulating factor; HGF, hepatocyte growth factor;

IL-4, interleukin-4; KEGG, Kyoto Encyclopedia of Genes and Genomes. (**G**) Genes in MP/DC cluster ranked according to log$_2$-fold changes [log$_2$(FC)] between seven patients with AFib and five controls. (**H**) Subclustering of 10,555 MP/DCs from five controls and seven patients with AFib. (**I**) Difference in abundance of cells belonging to MP/DC subclusters between seven patients with AFib and five control patients. Pie size indicates log$_2$(FC); color (blue, high; red, low) indicates the *P* value (two-tailed Student's *t* test). **P < 0.01. (**J**) Fraction of *SPP1*$^+$ macrophages in controls and patients with AFib. Bar graph shows mean ± SEM, *n* = 5 to 6 per group, two-tailed Student's *t* test. (**K**) Gene expression levels (represented by log-transformed normalized counts) across macrophage clusters; Kruskal-Wallis ($P < 2.2 \times 10^{-16}$) followed by two-tailed Wilcoxon rank sum test. ****Adjusted $P = 2 \times 10^{-16}$. (**L**) *SPP1* expression in MP/DCs from controls and patients with AFib.
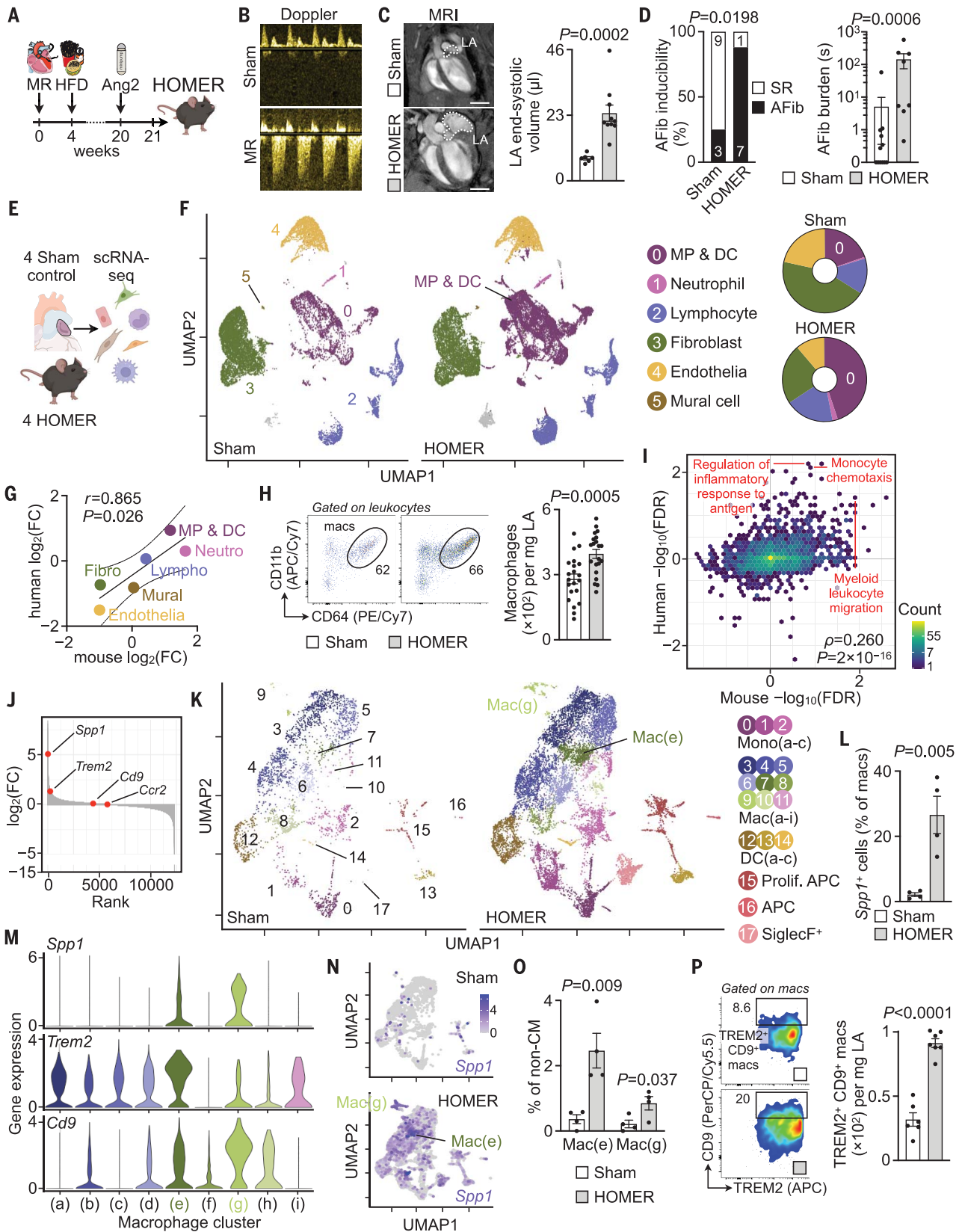
Fig. 2. Single-cell atlas of mouse atria. (**A**) HOMER mice are exposed to mitral valve regurgitation (MR), high-fat diet (HFD), and angiotensin 2 (Ang2). (**B**) Doppler of MR. (**C**) (Left) MRI of left atrium (LA). Scale bars, 3 mm. (Right) LA end-systolic volume, n = 6 to 10 per group from two independent experiments, two-tailed Mann-Whitney test. (**D**) AFib inducibility and burden. n = 8 to 12 per group from two independent experiments. (Left) Two-sided Fisher's exact test. (Right) Two-tailed Mann-Whitney test. Other parameters are shown in table S7. SR, sinus rhythm. (**E**) scRNA-seq was performed in four

sham and four HOMER mice. (**F**) (Left) UMAP. (Right) Cell population distributions. (**G**) Log$_2$(FC) of cell abundance in mouse and human atria. (**H**) Flow cytometry of sham and HOMER atria. $n = 21$ per group from five independent experiments, two-tailed Student's t test. APC/Cy7, allophycocyanin/cyanine 7; PE/Cy7, phycoerythrin/cyanine 7. (**I**) Scatterplot showing C5 GOBP GSEA species concordance. GSEA is performed on lists of genes ranked according to differential expression in the disease state. $-\log_{10}$(FDR) is plotted for mouse (x axis) and human (y axis). $-\log_{10}$ (FDR) are negative if the gene set is down-regulated. Yellow indicates high and blue indicates low gene set density. (**J**) Genes in MP/DC cluster ranked according to log$_2$ (FC) between four HOMER and four sham mice. The y axis was broken at -5 for

displaying the top down-regulated genes. (**K**) Subclustering of MP/DCs from four sham and four HOMER mice. APC, antigen-presenting cell. (**L**) Atrial *Spp1*+ macrophages by scRNA-seq. $n = 4$ per group, two-tailed Student's t test. (**M**) Gene expression levels (represented by log-transformed normalized counts) across macrophage clusters. (**N**) *Spp1* expression in MP/DCs from sham and HOMER mice. (**O**) *Spp1*+ subpopulations in sham and HOMER mice. $n = 4$ per group, two-tailed Student's t test. non-CM, noncardiomyocyte. (**P**) Flow cytometry of atrial macrophages in sham and HOMER mice. $n = 6$ to 7 per group from two independent experiments, two-tailed Student's t test. PerCP/Cy5.5, peridinin-chlorophyll-protein/cyanine 5.5. All bar graph data are mean ± SEM with individual values for data distribution.

cells also altered their gene expression (fig. S3 and data S3 and S4). Fibroblasts, for example, responded by up-regulating inflammatory pathways and matrix production (fig. S3C). In endothelial and mural cells, we observed up-regulation of genes indicative of ischemia and vascular remodeling (fig. S4).

Depending on their origin and microenvironment, macrophages and their subsets take on phenotypes that enable a range of diverging and even opposing functions (*3, 21*). To identify cell types that contribute to atrial remodeling, we examined atrial myeloid cells in detail. We reclustered MP/DCs, choosing a resolution that maximized the number of differentially expressed

genes between subclusters (fig. S5, A and B). Reclustering separated three monocyte subsets, an established number in human blood (*21*), and a fourth inflammatory monocyte cluster whose expression profile (fig. S5C and data S5) and uniform manifold approximation and projection (UMAP) position adjacent to macrophages (Fig. 1H) suggested an intermediate phenotype during monocyte-to-macrophage differentiation. At this resolution, we could distinguish five macrophage clusters (Fig. 1H, figs. S5C and S6, and data S6) and two DC clusters (Fig. 1H and fig. S5C). The inflammatory mono(b) cluster and the *SPP1*+ mac(c) cluster expanded 2.8- and 3.4-fold, respectively, in

diseased atria (Fig. 1I). The frequency of *SPP1*+ atrial cells increased in patients with AFib when compared with non-AFib controls (Fig. 1J). The expanding mac(c) cluster was the dominant *SPP1* source in atria of patients with AFib (Fig. 1, K and L); other immune and stromal cells did not express *SPP1* at high levels (fig. S7). *TREM2* and *CD9*, which encode proteins that can be detected by cell surface staining (*22*), further distinguished the *SPP1*+ mac(c) cluster from other cells (Fig. 1K and fig. S7). RNA in situ hybridization confirmed that macrophages express *SPP1* in atria of patients with AFib (fig. S8, A and B). Once secreted by macrophages, SPP1 associates with extracellular matrix (*13*).


Fig. 3. CCR2-dependent monocyte recruitment contributes to left atrial macrophage expansion and atrial disease.
(**A**) Flow cytometric quantification of recruited (YFP+ Td−) and locally sourced (YFP+ Td+) left atrial macrophages in *Cx3cr1*^CreER/+^*Ai9*^fl/+^ sham and HOMER mice. $n = 8$ to 12 per group from two independent experiments, two-tailed Student's t test. Td, tdTomato; YFP, yellow fluorescent protein. (**B**) Relative *Spp1* expression levels by qPCR in recruited (YFP+ Td−) and locally sourced (YFP+ Td+) left atrial macrophages in *Cx3cr1*^CreER/+^*Ai9*^fl/+^ HOMER mice. $n = 8$ per group from two independent experiments, two-tailed Wilcoxon matched-pairs signed-rank test. (**C**) Flow cytometric quantification of myeloid cell populations in left atrial tissues from C57BL/6 and *Ccr2*−/− HOMER mice. Macrophages: 21 C57BL/6 and 19 *Ccr2*−/− HOMER mice from five independent experiments; monocytes and neutrophils: 12 C57BL/6 and 10 *Ccr2*−/− HOMER mice from three independent experiments; two-tailed Student's t test. (**D**) Flow cytometric quantification of TREM2+ CD9+ left atrial macrophages in C57BL/6 and *Ccr2*−/− HOMER mice. $n = 7$ to 9 per group from two independent experiments, two-tailed Student's t test. (**E**) AFib inducibility and burden in C57BL/6 and *Ccr2*−/− HOMER mice by means of electrophysiological (EP) study. $n = 8$ to 9 per group from two independent experiments. (Left) Two-sided Fisher's exact test. (Right) Two-tailed Mann-Whitney test. Other EP parameters are shown in table S8. All bar graph data are mean ± SEM with individual values for data distribution.
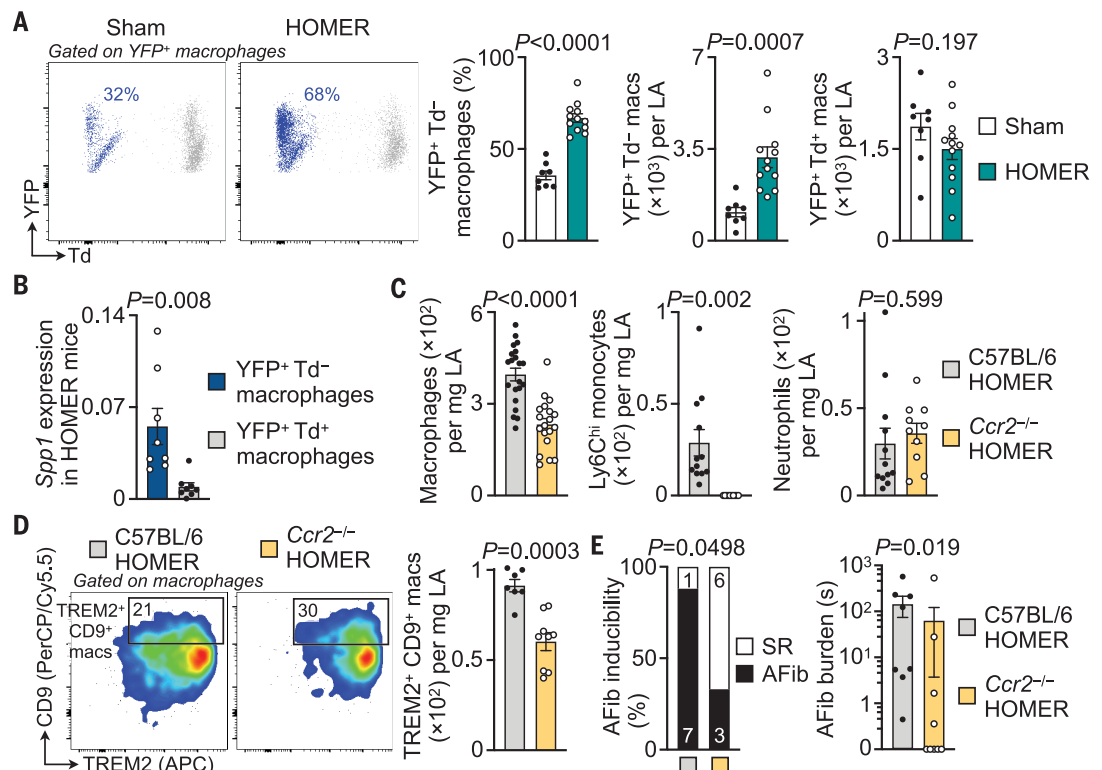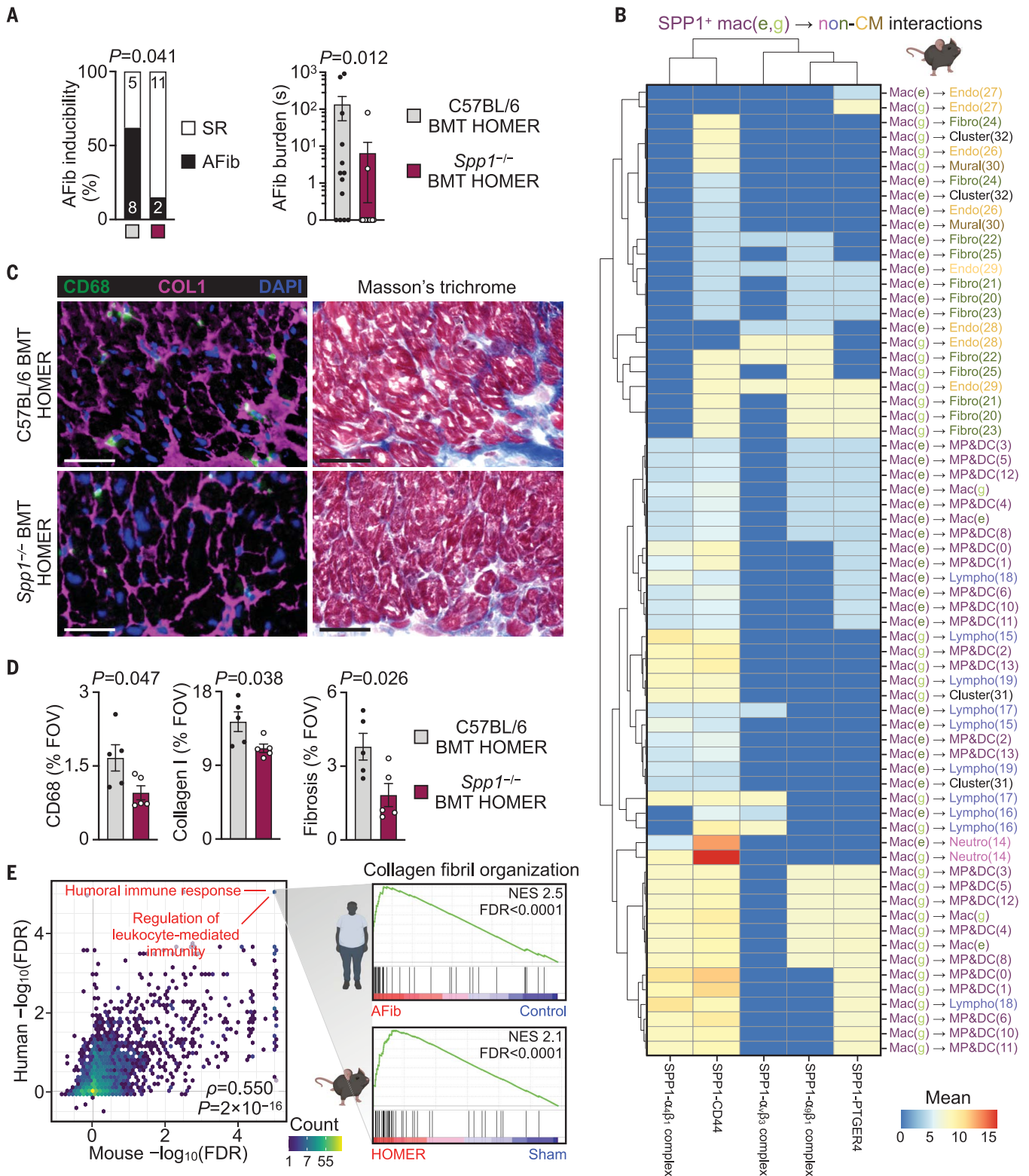
Fig. 4. Macrophage-derived SPP1 promotes atrial disease. (**A**) EP study of AFib inducibility and burden in C57BL/6 BMT HOMER and $Spp1^{-/-}$ BMT HOMER mice. $n = 13$ per group from three independent experiments. (Left) Two-sided Fisher's exact test. (Right) Two-tailed Mann-Whitney test. Other EP parameters are shown in table S9. (**B**) Heatmap of SPP1-receptor interactions between SPP1$^+$ macrophages [mac(e) and mac(g)] and other non-CMs in four HOMER mice. SPP1 and cognate receptors are shown on the x axis. Cell populations that

express $Spp1$ and the receptor are shown on the y axis and are color-coded according to the major cardiac cell types identified in Fig. 2F. Color of scale bar (red, high; blue, low) indicates average $Spp1$ and receptor expression levels in their respective interacting subpopulations (represented by mean normalized counts) if the enrichment of an interacting SPP1-receptor pair in the given interacting subpopulations was statistically significant ($P < 0.05$). Nonsignificant interactions were assigned a value of 0. (**C**) Representative immunofluorescent

staining of macrophages (CD68, green), collagen deposition (COL1, magenta), and nuclei [4′,6-diamidino-2-phenylindole (DAPI), blue] and histological staining of fibrosis (Masson's trichrome staining) in left atrial tissue from C57BL/6 BMT HOMER and $Spp1^{-/-}$ BMT HOMER mice. Scale bars, 50 μm. (**D**) Quantification of CD68$^+$, COL1$^+$, and fibrotic area in left atrial tissue from C57BL/6 BMT HOMER and $Spp1^{-/-}$ BMT HOMER mice. Bar graphs show percentage of positive staining per field of view (FOV); n = 5 per group from two independent experiments, two-tailed Student's t test. (**E**) Scatterplot showing concordance between C5 GOBP GSEA results in human and mouse fibroblasts in AFib and HOMER (as in Fig. 2I). (Inset) Detailed GSEA results for gene set "GOBP collagen fibril organization" in human and mouse fibroblast clusters. NES, normalized enrichment score. All bar graph data are mean ± SEM with individual values for data distribution.

Accordingly, immunofluorescence microscopy identified expanding colocalization of SPP1 protein with collagen in patients with AFib (fig. S8, C and D).

To explore atrial macrophage expansion in a larger cohort, we used immunofluorescence histology on left atrial appendages of 108 patients with AFib and/or mitral regurgitation and 41 controls in sinus rhythm (table S3). Atrial macrophages and their monocyte-derived CCR2$^+$ subset expanded most in patients with AFib and mitral regurgitation (fig. S8, E and F). In patients who had mitral regurgitation without AFib or AFib without mitral regurgitation, macrophages expanded to a lesser degree (fig. S8, E and F). In patients who had AFib without mitral regurgitation, AFib chronicity was less pronounced (table S3), which may explain why we observed fewer atrial macrophages in this cohort.

A mouse model of atrial disease

To dissect immune pathways involved in human AFib mechanistically, we used a mouse model that combined hypertension, obesity, and mitral valve regurgitation (HOMER) (Fig. 2A). Snaring the mitral valve to the ventricular wall produced mitral valve regurgitation (Fig. 2B). Mice consumed an obesogenic diet for 4 months, mirroring the risk that obesity engenders for AFib (23). Hypertension, also a risk factor for AFib, was induced with angiotensin 2 (fig. S9). The HOMER model elicited left atrial enlargement (Fig. 2C) commonly found in patients with AFib (24). HOMER mice developed increased AFib inducibility and burden compared with those of sham-operated normotensive control mice that consumed standard chow (hereafter referred to as controls) (Fig. 2D and fig. S10). Among individual HOMER components, obesity elicited the highest AFib inducibility, whereas mitral valve regurgitation enlarged atria the most (fig. S11). Spontaneous AFib episodes, which were monitored with electrocardiogram telemeters, were absent in HOMER mice. In HOMER hearts, left ventricles hypertrophied and dilated mildly, and left ventricular systolic function was slightly reduced (fig. S12A and table S4). Blood leukocyte counts, including Ly6C^{hi} monocytes, rose in HOMER mice (fig. S12, B and C). Histological analysis revealed more numerous macrophages, fibrosis, and collagen deposition in HOMER atria compared with those in controls (fig. S12, D and E), results that align with the fibrosis observed in patients with

AFib (25) and the effects of hypertension and metabolic stress on the ventricles (15, 26, 27). Hypertension and mitral valve regurgitation most clearly increased atrial macrophage numbers and fibrosis (fig. S13).

Replicating our human scRNA-seq pipeline by using left atrial tissues dissected from four HOMER mice and four control animals (Fig. 2E and fig. S14A), we successfully obtained 40,112 viable single cells, among which we identified the same cell types as in human atria (Fig. 2F; fig. S14, B and C; and table S5). The cellular composition changes in diseased atria correlated strongly between both species [Pearson's correlation coefficient (r) = 0.87] (Fig. 2G). We observed a twofold expansion of MP/DCs in HOMER mice similar to that in the human disease setting (Fig. 2F and table S5). Flow cytometry confirmed the HOMER-induced changes in the abundance of macrophages (Fig. 2H and fig. S15, A to C). Cardiac macrophage subsets can be distinguished by expression of CCR2 and major histocompatibility complex II (MHCII) (28, 29). In atria of HOMER mice, the number of CCR2$^+$ macrophages and monocytes rose (fig. S15, D and E).

We next examined the gene expression changes that occurred in MP/DCs of HOMER mice in relation to our human data. As before, we first performed GSEA on differentially expressed genes from a pseudo-bulk analysis comparing MP/DCs isolated from atria of HOMER or control mice. We then plotted the significance and direction of change for all Molecular Signatures Database (MSigDB) C5 (Gene Ontology) gene sets against the corresponding values in humans and found significant concordance between the two GSEA data sets [Spearman's rank correlation coefficient (ρ) = 0.26, $P < 2 \times 10^{-16}$] (Fig. 2I and data S7), indicating that the HOMER model recapitulated the pathway-level gene expression changes observed in patients. As in humans, $Spp1$ was among the top up-regulated genes in MP/DCs of HOMER atria (Fig. 2J). We then reclustered MP/DCs to obtain a higher-resolution view of these cells, choosing a resolution that separated three monocyte clusters [a number previously described in mouse blood (30)], nine macrophage clusters, three DC clusters, two antigen-presenting cell clusters, and one SiglecF$^+$ cell cluster (Fig. 2K). $Spp1^+$ cell frequencies increased in HOMER atria (Fig. 2L), a rise driven by the macrophage subpopulations mac(e) and mac(g) and not by other immune or stromal cells (Fig. 2, M and N, and fig. S16, A and B). In

close concordance with our human findings, $Spp1^+$ mac(e) and mac(g) clusters coexpressed $Trem2$ and $Cd9$ (Fig. 2M) and expanded in HOMER mice (Fig. 2, O and P, and fig. S16, C and D). Comparing MP/DC clusters across the two species (using the top 100 genes that distinguished each subcluster), we found that each human MP/DC cluster significantly matched at least one mouse cluster and that the human $SPP1^+$ cluster mac(c) was similar to the mouse $Spp1^+$ cluster mac(e) (fig. S17). This strong interspecies correlation is likely caused by similar risk factors in human patients and HOMER mice.

We next assayed contributions of individual HOMER components. $Ccr2$ was expressed highest in HOMER atria but also increased in hypertensive mice (fig. S18A). Atrial expression of $Csf1$, chemokines, adhesion molecules, inflammatory markers, and matrix increased the most in HOMER mice (fig. S18, B to F). $Spp1$ expression increased in HOMER mice but not after exposure to single components (fig. S18G). Thus, HOMER components have additive (for example, $Ccr2$ expression) and some synergistic effects (for example, $Spp1$ expression). Two of three HOMER components elicited intermediate atrial remodeling and $Spp1$ expression (fig. S19). Although combining all HOMER components reflected the risk factors present in our patient cohort most faithfully, further studies of single conditions (for example, metabolic consequences of high-fat diet on conducting cells) are warranted.

We then contrasted left atrial gene expression changes to the left ventricular myocardium. Unlike the atria, we observed no significant expansion of ventricular leukocyte frequencies in HOMER mice (fig. S20, A to C, and table S6). The decline of fibroblast frequencies that occurred in HOMER atria was absent in the ventricles (fig. S20, A to C, and table S6). Compared with ventricular cells, more genes changed in atrial myeloid cells and fibroblasts. For example, there were 1982 atrial but only 19 ventricular differentially expressed genes [with false discovery rate (FDR) < 0.05] in MP/DCs (with nine differentially regulated genes shared between the atria and ventricles) (fig. S20, D and E, and data S8). This pattern was inversed for endothelial cells, which had more differentially expressed genes in the ventricles than in the atria (fig. S20, D and E, and data S8). A principal components analysis revealed that in controls, atrial MP/DCs were located at a large distance from ventricular MP/DCs. The distance between atrial and ventricular MP/DCs

was less pronounced in HOMER mice (fig. S20F). We hypothesize that HOMER-induced activation of inflammatory programs equalizes some of the differences normally imprinted by the atrial versus the ventricular environment. That the HOMER model affects left ventricular leukocytes to a lesser degree than in the left atria corresponds with the more severe atrial than ventricular dilation observed with magnetic resonance imaging (MRI) (Fig. 2C and fig. S12A). The ventricular data reveal that hypertension, high-fat diet, and mitral valve disease affect not only atria but the entire heart, a notion reflected by the clinical association of AFib with heart failure (31).

The generation of the HOMER mouse and its scRNA-seq validation against patients with AFib provided us with a tool to assess whether immune cell expansion merely associates with—or alternatively, contributes to—AFib. We used the HOMER mouse for two follow-up studies that tested causal implications for key observations in patients with AFib: (i) expansion of inflammatory atrial macrophages and (ii) increased atrial SPP1 expression by those macrophages.

CCR2-dependent macrophage recruitment promotes AFib

Macrophage ontogeny often dictates function (32). For example, steady-state resident macrophages in the heart and brain are distinctly noninflammatory (33), whereas recruited infarct or stroke macrophages are inflammatory and damage tissues (34). We consequently sought to investigate macrophage origins in normal and diseased atria. Because atrial macrophages expand in diseased atria of HOMER mice (Fig. 2, F and H, and table S5) and enrich for the chemokine receptor CCR2 (fig. S15D), which recruited macrophages express (34), we combined the HOMER procedure with genetic fate mapping in $Cx3cr1^{CreER/+}Ai9^{fl/+}$ mice (fig. S21A). Although atrial macrophages were more likely to be derived from circulating monocytes than ventricular macrophages, most atrial macrophages were not sourced from monocytes in steady state (fig. S21B). In HOMER mice, recruitment expanded so that 67% of atrial macrophages derived from monocytes, a significant increase from the steady state (36%) (Fig. 3A). In line with increased atrial expression of $Csf1$ (fig. S18B) and up-regulation of the "Leukocyte proliferation" gene set by MP/DCs (fig. S21C), macrophage proliferation increased in HOMER atria (fig S21, D and E). Recruited macrophages in atria of HOMER mice were the primary source of $Spp1$, whereas locally sourced macrophages did not express this gene at high levels (Fig. 3B).

We used the HOMER procedure in $Ccr2^{-/-}$ mice to test the relevance of expanded macrophage recruitment for AFib. Blocking monocyte migration in $Ccr2^{-/-}$ HOMER mice decreased

blood monocyte, atrial Ly6C^{hi} monocyte, and macrophage expansion when compared with C57BL/6 HOMER mice, whereas other cell densities and blood pressure were unaffected (Fig. 3C and fig. S22, A to D). TREM2$^+$ CD9$^+$ macrophages were also lower in $Ccr2^{-/-}$ HOMER mice (Fig. 3D). Cardiac MRI revealed smaller left atrial volumes in $Ccr2^{-/-}$ HOMER mice (fig. S22E). $Ccr2^{-/-}$ HOMER mice exhibited lower AFib inducibility and AFib burden than those of C57BL/6 HOMER mice (Fig. 3E). Thus, macrophage recruitment expands during atrial remodeling, recruited macrophages highly express $Spp1$, and inhibiting macrophage recruitment reduces AFib.

To test whether CCR2 inhibition could alleviate established disease, we treated mice with the CCR2 antagonist CCL2-Fc (35) for 4 weeks after the last HOMER treatment component (fig. S23A). CCR2 inhibition reduced fibrosis in atria of HOMER mice (fig. S23, B and C). AFib inducibility and burden were lower in the treatment group, although this effect was not statistically significant (fig. S23D).

Macrophage-derived SPP1 is a pleiotropic AFib catalyst

Given that $Spp1$ is among the most up-regulated macrophage genes in AFib, we examined the causal role of this matricellular protein. We transplanted bone marrow from $Spp1^{-/-}$ mice into wild-type recipients ($Spp1^{-/-}$ BMT HOMER) to delete $Spp1$ in recruited macrophages (fig. S24, A and B). Wild-type recipients that received wild-type bone marrow and then underwent HOMER (C57BL/6 BMT HOMER) served as controls. Blood pressure and leukocyte counts were similar in both cohorts (fig. S24, C to E). Left atrial and ventricular volumes were preserved and left ventricular hypertrophy was lessened in mice in which $Spp1$ was deleted (fig. S24F). Deleting $Spp1$ in bone marrow–derived cells reduced AFib inducibility and AFib burden (Fig. 4A).

To outline mechanisms by which osteopontin exacerbates AFib, we investigated the crosstalk between $Spp1$-expressing macrophages and other atrial cells, using CellPhoneDB (36). In HOMER mice and patients with AFib, paracrine and autocrine interactions were found between macrophage-derived SPP1 and cognate SPP1 receptors expressed by immune and stromal cells (Fig. 4B and fig. S25). In HOMER mice, CellPhoneDB analysis implied SPP1$^+$ macrophage interactions with client cells via three integrins ($\alpha_4\beta_1$, $\alpha_v\beta_3$, and $\alpha_9\beta_1$), CD44, and prostaglandin E$_2$ receptor 4 (EP$_4$/PTGER4). These interactions, which included signaling to various macrophage and fibroblast clusters, suggested that SPP1 acts as a pleiotropic amplifier for atrial inflammation and fibrosis, which in turn contribute to an AFib substrate (37).

In support of this idea, the histology of atria collected from $Spp1^{-/-}$ BMT HOMER

mice showed fewer CD68$^+$ macrophages when compared with that of C57BL/6 BMT HOMER mice (Fig. 4, C and D), indicating that SPP1 may influence atrial macrophage supply. Atrial monocyte numbers were unchanged in $Spp1^{-/-}$ BMT HOMER mice (fig. S26A), making a role of SPP1 in monocyte recruitment unlikely. TUNEL (terminal deoxynucleotidyl transferase–mediated deoxyuridine triphosphate nick end labeling) and CD68 staining of atria indicated that macrophage death was also unchanged in the cohort in which $Spp1$ was deleted (fig. S26B). However, macrophage proliferation, which is up-regulated by HOMER conditions (fig. S21, D and E), declined in $Spp1^{-/-}$ BMT HOMER compared with that in C57BL/6 BMT HOMER mice (fig. S26, C and D). Thus, SPP1 augments atrial inflammation through increased macrophage proliferation.

Matrix production by fibroblasts increased in HOMER mice (S26, E and F), and immunoreactive α smooth muscle actin (αSMA) staining of HOMER atria documented an expansion of activated fibroblasts, which were reduced in $Spp1^{-/-}$ BMT HOMER mice (fig. S26, G to J). Atrial fibroblasts isolated from $Spp1^{-/-}$ BMT HOMER mice expressed less collagen than those from C57BL/6 BMT HOMER (fig. S26K). Furthermore, we detected reductions in collagen I deposition and Masson's trichrome staining in atria of $Spp1^{-/-}$ BMT HOMER mice (Fig. 4, C and D), which points to reduced fibroblast matrix production if these cells do not sense SPP1. This interaction may be particularly relevant because integrins—which, according to our CellPhoneDB analysis, fibroblasts use to sense SPP1—regulate fibroblast migration, proliferation, and activation, processes that precede increased tissue fibrosis (38, 39).

Comparing left atrial cells from $Spp1^{-/-}$ BMT HOMER with those from C57BL/6 BMT HOMER mice by means of scRNA-seq (fig. S27, A and B), we identified fibroblast clusters that expressed collagens at high levels (fig. S27, C to E). For these clusters, we pursued GSEA to examine through which pathways SPP1 activates atrial fibroblasts (fig. S27F). Fibroblast clusters from C57BL/6 BMT HOMER mice upregulated $Tgfb1$ gene sets. Inflammatory activation of fibroblasts by SPP1 was supported by the up-regulation of inflammatory gene sets in fibroblasts from C57BL/6 BMT HOMER when compared with $Spp1^{-/-}$ BMT HOMER mice (fig. S27F). Thus, SPP1 participates in inflammatory fibroblast activation partially through transforming growth factor–β (TGF-β) pathways. In atrial tissue from patients with AFib, SPP1 colocalization with collagen 1A1 expanded (fig. S8, C and D), lending further credence to SPP1 promotion of AFib through enhanced fibrosis.

To ascertain whether the transcriptional changes that occurred in atrial fibroblasts of HOMER mice are representative of alterations

in humans, we compared human and mouse fibroblast transcriptomes. We first performed GSEA (again using all C5 ontology MSigDB gene sets) on differentially expressed genes from a pseudo-bulk analysis comparing all fibroblast clusters isolated from atria of patients with AFib versus humans without AFib, as well as HOMER mice versus control mice. We then plotted the significance and direction of change for all gene sets for both species. Both GSEA data sets correlated strongly (Spearman's ρ = 0.55, $P < 2 \times 10^{-16}$) with gene sets related to immune response and collagen organization enriched in diseased atria (Fig. 4E and data S9). This pathway-level interspecies correlation further bolstered the physiological relevance of the HOMER model while also underscoring inflammation and fibrosis as central processes in AFib.

Discussion

In this study, we comprehensively assayed atria from patients and mice and documented large-scale shifts in the cellular frequencies and phenotypes during AFib. Macrophages expand more than any other cell type in AFib. Experiments in mice, in which either *Ccr2* or *Spp1* was deleted, demonstrated that targeting macrophages strengthens resilience against AFib (fig. S28).

In human and mouse atria, *SPP1* was among the top up-regulated macrophage genes. This matricellular protein, which increases in the blood of patients with AFib (*40*), stabilizes collagen (*41, 42*) and promotes fibrosis in hypertension (*43, 44*). We speculate that macrophage-derived SPP1 (*45*) augments atrial tissue heterogeneity and hinders conduction between cardiomyocytes. SPP1 signals to most other atrial cell classes, enhancing inflammation and fibrosis through interaction with various cell surface receptors. In the ventricular myocardium and in other organs, such signaling promotes myeloid cell activation and migration as well as extracellular matrix production by fibroblasts (*13, 15, 43, 44*). Thus, targeting SPP1 may have several distinctive effects that together preserve atrial conduction. The expanding numbers and altered phenotypes of atrial macrophages may have other disease-promoting consequences. For example, a loss of resident macrophages' relationships with cardiomyocytes (*46, 47*) may compromise atrial conduction.

Going forward, therapeutic strategies could target recruitment of inflammatory macrophages (CCR2) or macrophage-derived signals (SPP1). Macrophage-targeted therapy for atrial cardiomyopathy is most likely to succeed with concomitant normalization of risk factors—for example, through surgical valve repair, weight loss, and blood pressure management. Our data centrally position macrophages as targets for immunotherapy in patients with AFib.

REFERENCES AND NOTES

1. M. Litviňuková et al., Nature 588, 466–472 (2020).
2. J. A. Nicolás-Ávila, A. Hidalgo, I. Ballesteros, J. Leukoc. Biol. 104, 743–756 (2018).
3. E. Forte, M. B. Furtado, N. Rosenthal, Nat. Rev. Cardiol. 15, 601–616 (2018).
4. E. J. Benjamin et al., Circulation 139, e56–e528 (2019).
5. T. Yamashita et al., Circ. J. 74, 262–270 (2010).
6. N. Smorodinova et al., PLOS ONE 12, e0172691 (2017).
7. C. Yao et al., Circulation 138, 2227–2242 (2018).
8. Y. K. Iwasaki, K. Nishida, T. Kato, S. Nattel, Circulation 124, 2264–2274 (2011).
9. V. Rudolph et al., Nat. Med. 16, 470–474 (2010).
10. M. D. Robinson, D. J. McCarthy, G. K. Smyth, Bioinformatics 26, 139–140 (2010).
11. A. Subramanian et al., Proc. Natl. Acad. Sci. U.S.A. 102, 15545–15550 (2005).
12. P. Langfelder, S. Horvath, BMC Bioinformatics 9, 559 (2008).
13. N. G. Frangogiannis, Physiol. Rev. 92, 635–688 (2012).
14. I. F. Charo, R. M. Ransohoff, N. Engl. J. Med. 354, 610–621 (2006).
15. M. Hulsmans et al., J. Exp. Med. 215, 423–440 (2018).
16. N. V. Serbina, E. G. Pamer, Nat. Immunol. 7, 311–317 (2006).
17. X. Tang et al., Circulation 136, 2051–2067 (2017).
18. X. Liao et al., Proc. Natl. Acad. Sci. U.S.A. 115, E4661–E4669 (2018).
19. Q. Zhang et al., Nature 525, 389–393 (2015).
20. D. M. Hardbower et al., Proc. Natl. Acad. Sci. U.S.A. 114, E751–E760 (2017).
21. E. K. Koltsova, C. C. Hedrick, K. Ley, Curr. Opin. Lipidol. 24, 371–380 (2013).
22. P. Ramachandran et al., Nature 575, 512–518 (2019).
23. R. R. Huxley et al., Circulation 123, 1501–1508 (2011).
24. T. S. Tsang et al., Mayo Clin. Proc. 76, 467–475 (2001).
25. A. Xintarakou, S. Tzeis, S. Psarras, D. Asvestas, P. Vardas, Europace 22, 342–351 (2020).
26. J. D. Schilling, H. M. Machkovech, A. H. Kim, R. Schwendener, J. E. Schaffer, Am. J. Physiol. Heart Circ. Physiol. 303, H1366–H1373 (2012).
27. L. Wang et al., Eur. Heart J. 39, 1818–1831 (2018).
28. S. Epelman et al., Immunity 40, 91–104 (2014).
29. G. Bajpai et al., Nat. Med. 24, 1234–1245 (2018).
30. L. Ziegler-Heitbrock et al., Blood 116, e74–e80 (2010).
31. R. Gopinathannair et al., Circ. Arrhythm. Electrophysiol. 10.1161/HAE0000000000000078 (2021).
32. C. Blériot, S. Chakarov, F. Ginhoux, Immunity 52, 957–970 (2020).
33. F. F. Hoyer et al., Immunity 51, 899–914.e7 (2019).
34. S. Epelman, K. J. Lavine, G. J. Randolph, Immunity 41, 21–35 (2014).
35. C. D. Paavola et al., J. Biol. Chem. 273, 33157–33165 (1998).
36. M. Efremova, M. Vento-Tormo, S. A. Teichmann, R. Vento-Tormo, Nat. Protoc. 15, 1484–1506 (2020).
37. M. Harada, S. Nattel, Card. Electrophysiol. Clin. 13, 25–35 (2021).
38. K. Graf et al., Hypertension 35, 978–984 (2000).
39. V. Sarrazy et al., Cardiovasc. Res. 102, 407–417 (2014).
40. J. Molvin et al., Open Heart 7, e001190 (2020).
41. L. Liaw et al., J. Clin. Invest. 101, 1468–1478 (1998).
42. S. R. Künzel et al., Circ. Res. 129, 804–820 (2021).
43. A. R. Collins et al., J. Am. Coll. Cardiol. 43, 1698–1705 (2004).
44. Y. Matsui et al., Hypertension 43, 1195–1201 (2004).
45. B. López et al., Cardiovasc. Res. 99, 111–120 (2013).
46. J. A. Nicolás-Ávila et al., Cell 183, 94–109.e23 (2020).
47. M. Hulsmans et al., Cell 169, 510–522.e20 (2017).
48. M. Ashburner et al., Nat. Genet. 25, 25–29 (2000).
49. S. Carbon et al., Nucleic Acids Res. 49 (D1), D325–D334 (2021).
50. A. Liberzon et al., Cell Syst. 1, 417–425 (2015).

SUPPLEMENTARY MATERIALS

science.org/doi/10.1126/science.abq3061
Materials and Methods
Figs. S1 to S28
Tables S1 to S11
References (*51–67*)
Data S1 to S9
MDAR Reproducibility Checklist

View/request a protocol for this paper from *Bio-protocol*.

Recruited macrophages elicit atrial fibrillation

Maarten Hulsmans, Maximilian J. Schloss, I-Hsiu Lee, Aneesh Bapat, Yoshiko Iwamoto, Claudio Vinegoni, Alexandre Paccalet, Masahiro Yamazoe, Jana Grune, Steffen Pabel, Noor Momin, Hana Seung, Nina Kumowski, Fadi E. Pulous, Daniel Keller, Constanze Bening, Ursula Green, Jochen K. Lennerz, Richard N. Mitchell, Andrew Lewis, Barbara Casadei, Oriol Iborra-Egea, Antoni Bayes-Genis, Samuel Sossalla, Chin Siang Ong, Richard N. Pierson, Jon C. Aster, David Rohde, Gregory R. Wojtkiewicz, Ralph Weissleder, Filip K. Swirski, George Tellides, George Tolis, Jr., Serguei Melnitchouk, David J. Milan, Patrick T. Ellinor, Kamila Naxerova, and Matthias Nahrendorf

Editor's summary

Atrial fibrillation (AFib), the most common type of heart arrhythmia, is a serious condition that can result in atrial blood clots and thromboembolic stroke. Hulsmans *et al.* performed single-cell RNA sequencing on atrial tissue from AFib patients and healthy controls to better understand how stromal and immune cells contribute to this disease. They found that recruited CCR2+ SPP1+ macrophages expanded in AFib patients. These cellular and transcriptomic changes were recapitulated in a mouse model of AFib that integrated hypertension, obesity, and mitral valve regurgitation (HOMER). Disrupting *Ccr2*, which coordinates inflammatory macrophage recruitment to atria, or *Spp1*, which helps to drive inflammatory fibroblast activation by macrophages, ameliorated disease burden in HOMER mice, suggesting two potential immunotherapy targets for Afib patients. —STS

View the article online
https://www.science.org/doi/10.1126/science.abq3061
Permissions
https://www.science.org/help/reprints-and-permissions

Use of this article is subject to the Terms of service